Proceedings World Geothermal Congress 2023
Beijing, China, April 17 – 21, 2023

A Probabilistic Methodology for Evaluating Fluid Injection-induced Seismic Risk in Faulted Geothermal Reservoirs and Application to a Field Case Study in Iceland

Wenzhuo Cao[a], Sevket Durucan[a], Ji-Quan Shi[a], Anna Korre[a], Thomas Ratouis[b], Vala Hjörleifsdóttir[b]

[a] Department of Earth Science and Engineering, Royal School of Mines, Imperial College London, London, SW7 2AZ, United Kingdom; [b] Orkuveita Reykjavíkur (OR-Reykjavík Energy), Bæjarhálsi 1, 110 Reykjavik, Iceland

Corresponding author: w.cao15@imperial.ac.uk

Keywords: induced seismicity; fluid injection; fracture criticality; probabilistic seismic risk evaluation; geothermal systems

ABSTRACT

Fault re-activation and associated seismicity pose a potential threat to industrial processes involving fluid injection into the subsurface. This paper presents the development of a probabilistic methodology to evaluate fluid injection-induced seismic susceptibility in faulted reservoirs. This methodology assumes that fluid injection-induced seismicity results from slippage of pre-existing fractures primarily driven by fluid pore pressure diffusion. The fracture criticality, defined in this study as the gradient of critical fluid pressure change to trigger seismicity ($\Delta p_c/h$, h being the reservoir depth), is used as the metric for fault slip susceptibility in the evaluation. The probabilistic injection-induced seismic risk evaluation is carried out by integrating seismic observations and hydrogeological modelling of fluid injection operations to obtain the probabilistic distribution of fracture criticality, which is in turn used to calculate the likelihood of seismic event occurrence within a certain region during a fluid injection period. The proposed seismic risk evaluation method considers the injection-driven fluid pressure increase, the variability of fracture criticality, and regional fracture density. Utilising this methodology, the probabilistic distribution of fracture criticality was obtained to evaluate the potential for injection-induced seismicity in both fault and off-fault zones at the Hellisheiði geothermal site, Iceland over a two-year period. Fault zones around five geothermal fluid re-injection wells at the site were estimated to have relatively high probability of seismic event occurrence, and these regions experienced high levels of induced seismicity over the microseismic monitoring period. The seismotectonic state estimated for each zone is generally consistent with the forecasted susceptibility to seismicity based on statistics of fracture criticality.

1. INTRODUCTION

Induced seismicity assessment is a key component to inform seismic hazard evaluation (seismicity that has the potential to cause damage) and seismic risk (the probability of unfavourable consequences of seismic hazards on humans and their built environment) (Schultz et al., 2021). This requires a thorough understanding of conditions under which seismic events are induced by fluid injection. A rigorous analysis of susceptibility to injection-induced seismicity involves careful examination of three different aspects involved: (1) hydrological and geomechanical response of subsurface reservoirs under injection conditions; (2) heterogeneous distribution of pre-existing fractures in the subsurface, which are difficult to directly detect and characterise; and (3) natural variability of fracture attributes and rock properties, which can result in the variability of fluid pressure perturbations required to trigger seismicity. Although fracture slippage in the subsurface is governed by the deterministic Mohr-Coulomb slippage criterion, the intrinsic variability of rock properties and fracture attributes inevitably brings about stochasticity in the seismic generation process.

Hydrogeological modelling addresses the first aspect by representing the deterministic physical process from a mechanics perspective, which forms the basis for physics-based seismic evaluation methods (Grigoli et al., 2017; Zhang et al., 2013). Besides outcrop fracture mapping and geological structure characterisation, observations of microseismicity, which result from the slippage of a subset of underlying pre-existing fractures, also provide useful information regarding the spatial distribution and density of fractures, and thus contribute to the understanding of the second aspect (Fisher et al., 2004; Zhao et al., 2019). Probabilistic assessment of induced seismicity proves an effective tool to address the third aspect by quantifying uncertainties involved in the seismic generation process (Rothert and Shapiro, 2007; Walsh III and Zoback, 2016). The integrated analysis of seismic observations and hydrogeological modelling allows for quantifying the variability of perturbations required to trigger seismicity, thus providing a probabilistic perspective in evaluating the susceptibility to injection-induced seismicity. However, there are few induced seismicity evaluation methods reported in the literature that incorporate seismic observations, hydrogeological modelling and probabilistic seismicity occurrence analysis.

This paper presents work carried out on the development and application of a probabilistic seismic susceptibility evaluation framework by combining seismic observations and hydrogeological modelling of fluid injection operations in faulted reservoirs. Fracture criticality, defined here as the gradient of critical fluid pressure change to trigger seismicity ($\Delta p_c/h$), is used as a metric of fracture slip susceptibility in the probabilistic evaluation. This evaluation framework is demonstrated using induced seismicity data recorded during a 2-year fluid re-injection period (15 April 2020 - 15 April 2022) at the Hellisheiði geothermal field, Iceland. During the probabilistic evaluation, the induced seismicity data was grouped in six-month intervals for analysis. Starting from the first six-month period, the induced seismicity data was analysed and spatially correlated with major fault structures. Hydrogeological simulations were then conducted to represent the hydrological response to the fluid injection over the same re-injection period. The integrated interpretation of fracture criticality was performed for each fault zone, which was then used to provide probabilistic injection-induced seismic hazard maps for the next six-month period at the site.

2. A SEISMIC SUSCEPTIBILITY EVALUATION METHOD BASED ON STATISTICS OF FRACTURE CRITICALITY

Slippage of pre-existing fractures has been recognised as the dominant mechanism for fluid injection-induced seismicity (e.g., Elsworth et al., 2016). In this respect, the susceptibility to fluid injection-induced seismicity can be evaluated in terms of the fracture slip susceptibility. For any selected measure of fracture slip susceptibility, the slippage of each individual pre-existing fracture is characterised by a critical value, according to the Mohr-Coulomb fracture slippage criterion. When this measure of fracture slip susceptibility is independent of reservoir depth, the statistical distribution of its critical values for a set of slipped fractures represents only uncertainties inherent in the fracture slippage process, which could be used for probabilistic forecasting of future seismicity. Based upon this understanding, a probabilistic seismic susceptibility evaluation method that integrates recorded seismicity interpretation and hydrogeological modelling is developed to estimate the seismicity occurrence probability.

2.1 Fracture criticality as a metric of fracture slip susceptibility

To account for uncertainties intrinsic to the fracture slip process, the fracture slip susceptibility index used for probabilistic evaluation of induced seismicity needs to meet the following requirements: 1) critical value to trigger fracture slippage is independent of reservoir depth, and 2) statistics of the critical value reflects uncertainties in both tectonic stress gradients and fracture frictional properties. Conventional indices, such as the fluid pressure p, fluid pressure change Δp and the Coulomb failure stress change ΔCFS, being generally depth-dependent, fail to meet the two requirements. To this end, the gradient of fluid pressure change $\Delta p/h$ was proposed as a reservoir depth-independent metric of fracture slip susceptibility. Critical values for this index can be expressed as a constant value related to both tectonic stress gradients and fracture frictional properties, therefore, this index meets both the requirements and is able to characterise the perturbations required to trigger seismicity. The lower is $\Delta p_c/h$, the more critical the pre-existing fracture.

$\Delta p_c/h$ for induced seismicity recorded (or pre-existing fractures that undergo slippage) is also easy to obtain by integrating microseismic observations and hydrogeological simulation as discussed later. The gradient of fluid pressure change $\Delta p/h$ is used as the metric of fracture slip susceptibility in probabilistic seismic susceptibility evaluation in this work. For convenience, the gradient of critical fluid pressure change $\Delta p_c/h$ is defined as fracture criticality C.

2.2 Seismic susceptibility evaluation based on statistics of fracture criticality

Owing to the inherent heterogeneity of tectonic stresses, fracture attributes (such as fracture orientation) and rock properties (such as friction coefficient), the criticality ($C = \Delta p_c/h$) of a random set of fractures subjected to fluid injection may vary in a range ($C_{min} \sim C_{max}$), even within the same host rock. The probability for an individual pre-existing fracture to satisfy Mohr-Coulomb fracture slippage criterion equals to the probability of the prevailing gradient of fluid pressure change ($\Delta p/h$) being greater than the fracture criticality. Considering that the fracture criticality is statistically distributed, the probability can be expressed as (Shapiro, 2015):

$$P_f = \int_0^{\Delta p/h} f(C)\,\mathrm{d}C \tag{1}$$

where $f(C)$ is the probability density function (PDF) of the fracture criticality $C(r)$ at any spatial location r. Given the observed range for the fracture criticality ($C_{min} \sim C_{max}$), the seismic occurrence probability would be 0 when $\Delta p/h < C_{min}$, and 1 when $\Delta p/h > C_{max}$.

In the case of the simplest possible PDF for the fracture criticality, i.e., the uniform PDF where $f(C) = 1/(C_{max} - C_{min})$ = constant ($C_{min} \le \Delta p/h \le C_{max}$), the seismic occurrence probability can be simplified as a linear function of $\Delta p/h$:

$$P_f = \frac{\Delta p/h - C_{min}}{C_{max} - C_{min}} \quad (C_{min} \leqslant \Delta p/h \leqslant C_{max}) \tag{2}$$

Considering the evaluation of seismic susceptibility in one gridblock, the probability of seismic event occurrence within this particular gridblock region can be expressed as a function of the probability for an individual fracture to satisfy the Mohr-Coulomb fracture slippage criterion P_f, and the regional fracture density d within the gridblock region:

$$P = \begin{cases} P_f d & d \leqslant 1 \text{ per gridblock} \\ 1 - (1 - P_f)^d & d > 1 \text{ per gridblock} \end{cases} \tag{3}$$

The injection-induced seismic susceptibility evaluation described above can be performed for injection field sites containing various geological structures or stratigraphical formations. Key assumptions of the seismic evaluation method include: (1) a random set of pre-existing fractures as hypocentres of induced seismicity is considered to be statistically homogeneously distributed within each geological structure or stratigraphical formation; (2) pre-existing fractures within different geological structures or stratigraphical formations are characterised by different fracture attributes (such as fracture density and fracture criticality); (3) fractures are orientated parallel to the regional fault strike, and the fracture density is proportional to the density of field monitored seismicity (Cao et al., 2020a, 2020b); and (4) pre-existing fractures do not mutually interact.

The evaluation starts with *the zonation of geological structures* in the region of investigation. The areal extent of geological structures (e.g., fault zones) is identified based on available data, including structure models for fault systems, outcrop fracture mapping, and historical seismic clustering observations. From the start of fluid injection operations, *a sequence of fluid injection parameters (such as injection rate and wellhead pressure) and concurrent seismic catalogue are recorded* and *divided into sequential periods*. The evaluation involves *integrated seismic and hydrogeological analysis for each period*, and *probabilistic forecasting of seismicity for the next period*. This evaluation process, besides the comparison between recorded seismicity and probability forecasts, is iterated for each period until the end of fluid injection operations.

The procedure for probabilistic forecasting through integration of microseismic observations and hydrogeological simulation comprises the following steps:

Step 1, *analysis of field monitored induced seismicity within the period considered* is performed. 3D hypocentre coordinates of recorded seismicity are used to filter ones falling within the region corresponding to the reservoir model domain. Each recorded seismic event within a specified distance to known geological structures is assigned to the nearest one. The fracture density in each geological structure is inferred from the density of induced seismicity falling within this zone.

Step 2, *hydrogeological modelling of reservoir response to fluid injection* is carried out. To ensure the reservoir behaviour to be realistically represented, the reservoir model constructed would incorporate known geological structures and be calibrated through historically matching field injection pressure time series over the injection period according to field injection rates. The fluid pressure change Δp at the hypocentre of each recorded seismic event at the time of seismic occurrence is considered as the critical fluid pressure change Δp_c to trigger the event, and is extracted from the calibrated reservoir model. The fracture criticality $\Delta p_c/h$ is then calculated for each induced seismic event.

Step 3, *estimation of the susceptibility to seismicity occurrence based on the statistics of fracture criticality* is achieved. The histograms of the fracture criticality, representing its probability density, can be obtained for each individual geological structure, or collectively by aggregating all possible values. Based on modelled fluid pressure change Δp throughout the model domain for the next period, the likelihood that the Mohr-Coulomb fracture slippage criterion is satisfied at any spatial location for the next period can be calculated according to Equation (1). Combining the fracture density obtained in Step 1, the likelihood of seismic event occurrence within each gridblock throughout the model domain for the next period is estimated according to Equation (3). A flow chart of the procedure for the seismicity occurrence probability forecasting is presented in Figure 1.

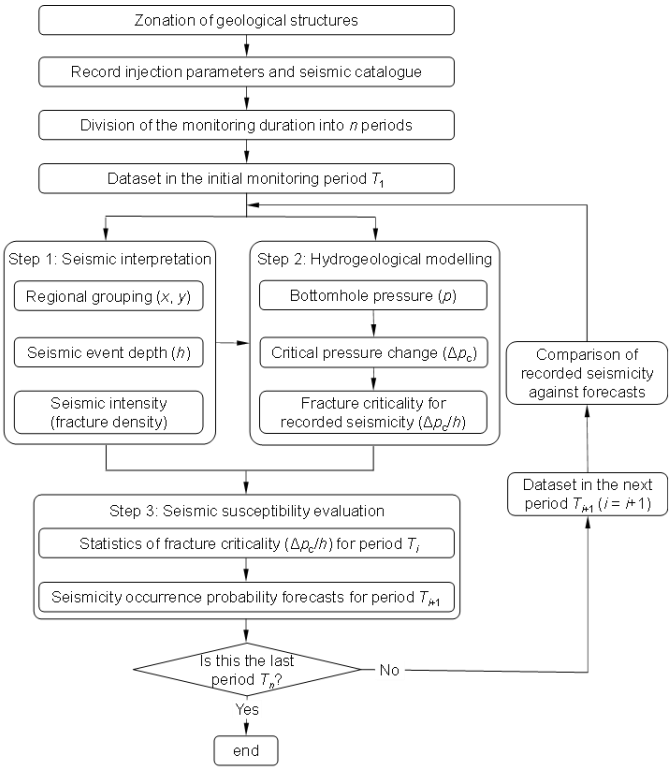

Figure 1: Procedure for probabilistic fluid injection-induced seismicity forecasting using integrated monitored seismicity interpretation and hydrogeological modelling.

3. GEOTHERMAL FLUID RE-INJECTION AT HELLISHEIÐI GEOTHERMAL FIELD

Located in the Southwest Iceland, the Hellisheiði geothermal field is one of the largest geothermal fields in the country, producing geothermal fluid at 240-320 °C from a subsurface reservoir at depths ranging from 1.5 to 3.3 km. The Hellisheiði geothermal heat and power plant, operated by Orkuveita Reykjavíkur (Reykjavik Energy), started production in 2006, and the current installed capacity is 303 MWe for power generation and 200 MWth for space heating.

The general stratigraphy at Hellisheiði comprises of alternating successions of hyaloclastite formations formed during glacial periods and lava sequences from interglacial periods. The region has a complicated tectonic setting, consisting of NNE-SSW trending extensional fault structures with sub-vertical dips and highly fractured fissure swarms (Ratouis et al., 2019) (Figure 2). Faults in the Hellisheiði region are normal faults, whilst faults in the South Iceland Seismic Zone are mostly strike slip faults with N-S orientation (Gunnarsson, 2013). The maximum horizontal principal stress follows a NNE orientation, aligned with the strike of major faults.

Operation permits require all geothermal brine after production to be re-injected back to the geothermal reservoir. Re-injection of the geothermal brine and condensate takes places in two distinct sites. The main re-injection site, the Húsmúli area, is located on the north-western edge of the field, and annually re-injects around 12 Mt of geothermal spent fluid through five boreholes (HN09, HN12, HN14, HN16 and HN17). The re-injection wells at Húsmúli target major fault structures: the fault F1 cuts across well trajectories of HN14 and HN17, the fault F3 cuts across those of HN09, HN14, HN16 and HN17, and the fault F4 cuts across those of HN09, HN12, HN16 and HN17 (Figure 2). Wells are cased off down to ~800 m depth to obstruct the loss of circulation fluid. Fluid re-injection into wells HN09, HN12, HN14 and HN17 started on 1 September 2011, followed by the well HN16 on 23 September (Juncu et al., 2020).

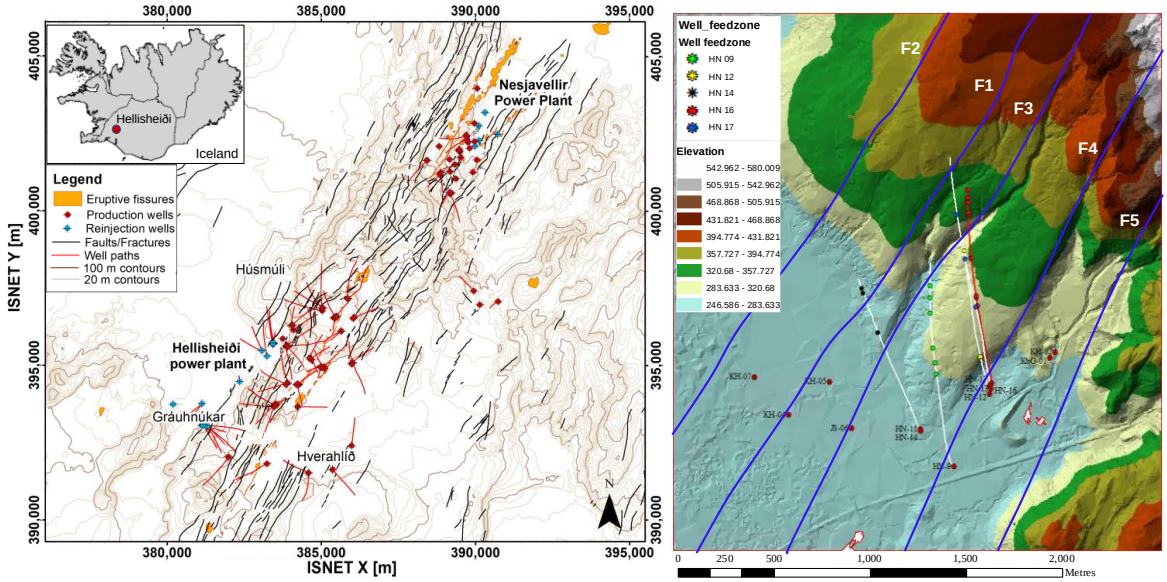

(a) (b)

Figure 2: (a) Map of the Hengill volcano and the Hellisheiði and Nesjavellir geothermal fields showing elevation contours, surface faults/fractures, and main production and re-injection wells and well paths projected to the surface (after Tómasdóttir 2018). (b) Map of the Húsmúli area showing the location of five geothermal fluid re-injection wells (HN09, HN12, HN14, HN16 and HN17) and five fault structures (F1- F5).

4. SEISMIC SUSCEPTIBILITY EVALUATION BASED ON STATISTICS OF FRACTURE CRITICALITY AT HELLISHEIÐI GEOTHERMAL FIELD

Fluid injection operational data and concurrent seismic catalogue during a 2-year period between 15 April 2020 and 15 April 2022 at the Hellisheiði geothermal field were used to demonstrate the induced seismicity susceptibility evaluation method based on statistics of fracture criticality. The seismic catalogue was kindly provided to the authors by the COSEISMIQ project. This seismic catalogue was divided into four sequential six-month periods, such that integrated microseismic interpretation and hydrogeological modelling over early periods could be used to provide seismic occurrence forecasts over subsequent ones. Sections 4.1-4.3 showcase the field microseismic data analysis, hydrogeological modelling of concurrent geothermal fluid re-injection, and probabilistic seismic evaluation for the first six-month period (between 15 April and 15 October 2020), which provides seismic occurrence forecasts over the second six-month period (between 16 October 2020 and 15 April 2021). Section 4.4 presents the six-month seismicity occurrence probability forecasts for four six-month periods and comparison against recorded seismicity when seismic records are available.

4.1 Geothermal fluid re-injection induced seismicity

Induced seismic activities were persistently occurring at Húsmúli during 15 April – 15 October 2020, totaling at 975 recorded seismic events. Figure 3 presents the spatial distribution of induced seismicity over the period of investigation at the Húsmúli area. The depth of induced seismic events shows significant variation, ranging from close to the ground surface down to over 6 km depth. A large proportion of the seismic events are located in the vicinity of major fault structures. Whilst induced seismicity went through a quiescence period during 16 May – 15 July (Figure 3b, c), they were relatively active over the remaining period (Figure 3a, d, e, f). The largest seismicity swarm generally located in the vicinity of major faults, shifting from the F1 fault zone during 15 April – 15 May (Figure 3a), to the F2 fault zone during 16 July – 15 September (Figure 3d,e), and back to the F1 fault zone during 16 September – 15 October (Figure 3f). This marked volatility in spatial and temporal seismic characteristics were also reflected in historical seismic observations between September 2011 and May 2012 at the same field site (Juncu et al., 2020).

Out of all the events recorded during 15 April and 15 October 2020 at Húsmúli, a total of 718 seismic events were identified to locate within the reservoir model domain as discussed later in the following Sections. Each seismic event within 200 m distance to the major faults was assigned to the closest fault. The remaining seismic events (those located at off-fault zones) were categorised as a separate group. Whilst 623 seismic events (86.8%) were associated with faults, 95 events (13.2%) located at off-fault zones.

4.2 Hydrogeological modelling of geothermal fluid re-injection at Hellisheiði

A reservoir model of a part of the Húsmúli area measuring 6 km × 5 km × 3 km (northing length × easting length × height) was constructed in the industry standard reservoir simulator ECLIPSE 300 to simulate the reservoir response of the five major faults and surrounding areas to fluid re-injection from the five re-injection wells over the period 15 April – 15 October 2020. The gridblock dimension of the model is 100 m in all the three directions.

The reservoir model constructed was based on a geological model of the Hellisheiði geothermal field, which incorporated surface mapping data, well data, well logging data, geophysics data, and laboratory analyses data (Gunnarsdóttir and Poux, 2016). The geological model is comprised of a combination of a lithological model and a structural model. The reservoir model developed consists of two main types of geological formations, the hyaloclastic formation (mostly at 0-~1600 m depth) and basalt basement (mostly at ~1600-3,000 m depth). Five fault structures (F1-F5), which represent planes of crustal weakness and fracturing resulting from intrusions and fissure eruptions, were incorporated in the reservoir model. Digitised from the geological model, these faults were extended to the surface to fit the surface fault map, and down to 3 km depth to allow fluid flow at varying depths.

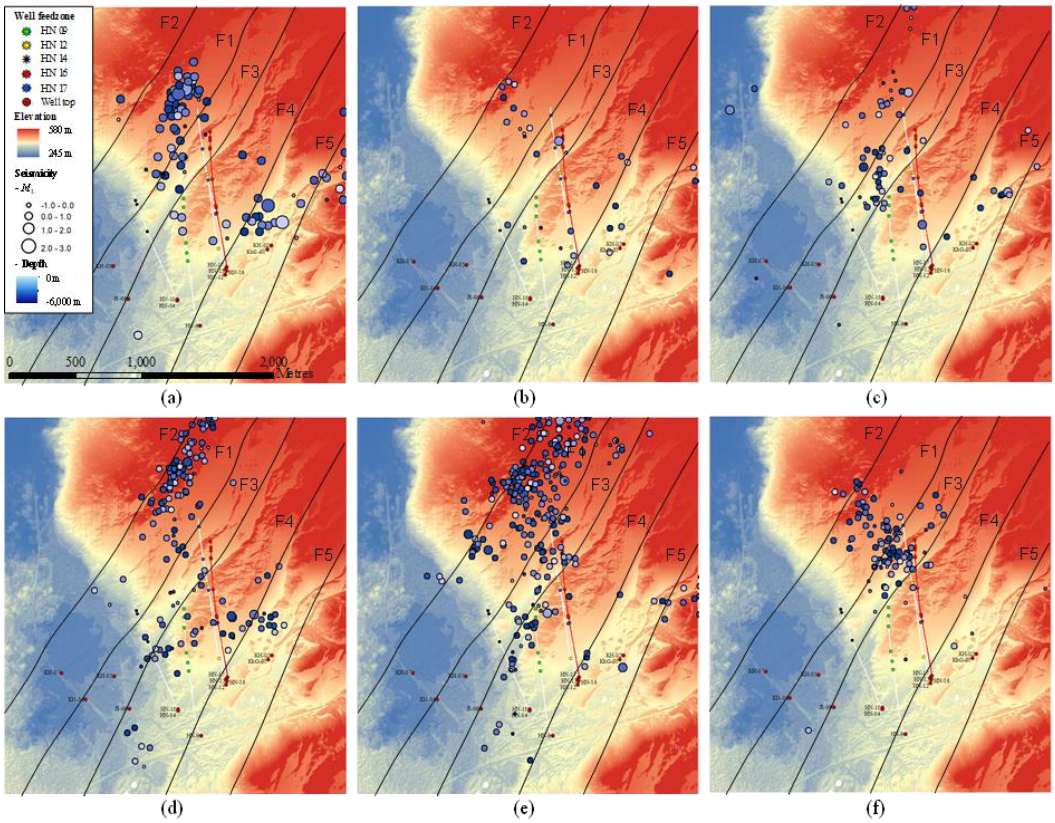

Figure 3: Spatial distribution of monitored induced seismicity at the Húsmúli area during: (a) 15 April – 15 May, (b) 16 May – 15 June, (c) 16 June – 15 July, (d) 16 July – 15 August, (e) 16 August – 15 September, and (f) 16 September – 15 October, 2020.

Both the reservoir and basement formations in the model domain were assumed to have uniform reservoir properties (porosity and permeability) for simplicity. According to the analysis carried out on 80 samples of basaltic hyaloclastic tuffs (Frolova et al., 2004; Snæbjörnsdóttir et al., 2014), the hyaloclastic formation as a reservoir manifests broad variations in both porosity and permeability, varying in the range of 0.14-0.57 and 0.001-6,400 mD, respectively. In this work, the porosity value of the reservoir formation was set to 0.10, while the permeability values for the reservoir formation and the faults were determined from history matching the bottomhole pressure time series over the period of investigation. The combination of a permeability of 60 mD for the reservoir formation, and a much higher permeability of 60 Darcy for the faults were found to provide a reasonable match for the five re-injection wells (Figure 4). The basalt basement was assigned a porosity of 0.08 and a permeability of 3.75 mD, following Snæbjörnsdóttir et al. (2018) and Cao et al. (2022). A pore volume multiplier of 10,000 was applied to the lateral boundaries of the reservoir model to account for the large volume of pore space surrounding the model domain.

The geothermal reservoir model was first initialised to hydrostatic conditions with the in-situ overpressure. According to field injection rate and pressure time series, fluid circulation in the geothermal reservoir at the Húsmúli area had already been established before the modelling started, and fluid flow has maintained a quasi-steady-state condition throughout the modelling period. Therefore, the hydrological effect from the previous decade of fluid injection since 2011 is considered to have limited influence on the model results. Nevertheless, a pre-modelling step, accounting for fluid injection over a month's period before 15 April 2020, was then simulated so as to establish fluid circulation in the geothermal system.

The history matching efforts attempted to match bottomhole pressures for all five injection wells at the same time. Figure 4 presents the history matching results for the five re-injection wells at the Húsmúli area. The modelled and field injection bottomhole pressures achieve a fairly close match over the period of investigation, indicating that the fluid pressure field obtained from this reservoir model could represent the critical fluid pressure to induce seismicity at the Húsmúli area. It is noted that pressure time series for well HN16 are characterised by more fluctuations than others, likely due to the concurrent CO_2 injection at this well, which was not considered in the hydrogeological modelling.

4.3 Probabilistic seismic susceptibility evaluation of faulted rocks at Hellisheiði

Figure 5 presents the histograms of critical fluid pressure change and gradient of critical fluid pressure change (fracture criticality) for induced seismicity recorded during 15 April – 15 October 2020 at different areas. Histograms of both variables follow Gaussian distribution with the similar shape and spread. The critical fluid pressure change for induced seismicity at each area reflects the prevailing fluid pressure increase within the corresponding fault. Both critical fluid pressure change and fracture criticality are higher for induced seismicity close to the injection wells and lower for those away from the wells. The fracture criticality is generally below 0.3 bar/km at off-fault zones, spanning from 0.001 to 0.5 bar/km at F1, F2 and F5 fault zones, and reaching up to 1.0 bar/km at F3 and F4 fault zones.

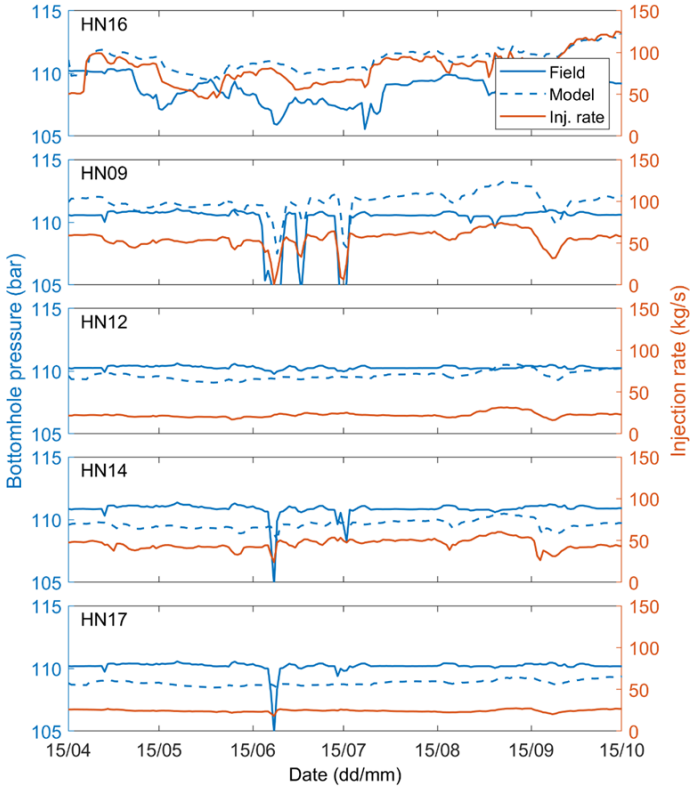

Figure 4: Geothermal fluid injection rates and history matching of field bottomhole pressure time series at 5 re-injection wells at the Húsmúli area during 15 April – 15 October 2020.

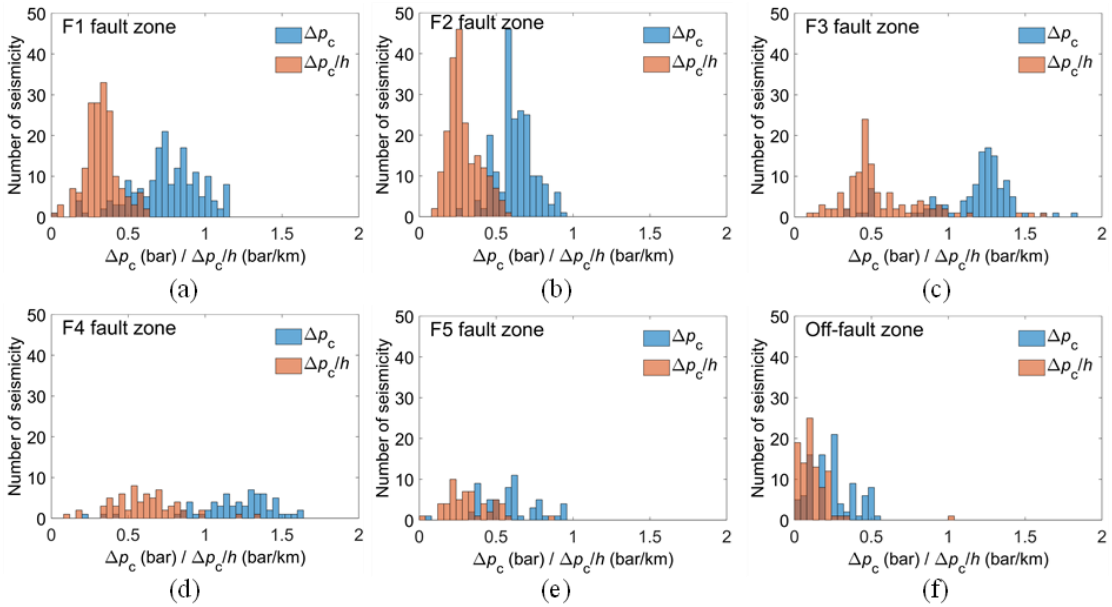

Figure 5: Histograms of critical fluid pressure change Δp_c and gradient of critical fluid pressure change $\Delta p_c/h$ (fracture criticality) for induced seismicity recorded at different areas at Húsmúli during 15 April – 15 October 2020: (a) F1 fault zone, (b) F2 fault zone, (c) F3 fault zone, (d) F4 fault zone, (e) F5 fault zone, and (f) off-fault zone.

Figure 6 presents probabilistic seismic susceptibility estimation results for the second six-month re-injection period at 1 km depth at the Húsmúli area. As shown in Figure 6(a), the modelled re-injection-induced fluid pressure increase is around 2 bar surrounding the five re-injection wells, and it decreases away from the wells. Largely dictated by the major faults, the contours of fluid pressure change are predominantly orientated in alignment with the fault strike. There are also local extensions of the contour boundary around the faults, resulting from larger elevated fluid pressure changes due to the higher permeability of faults. Owing to quasi-steady-state fluid flow conditions reached at the Húsmúli area, the spatial distribution of fluid injection-induced pressure change is maintained almost constant over the period of investigation.

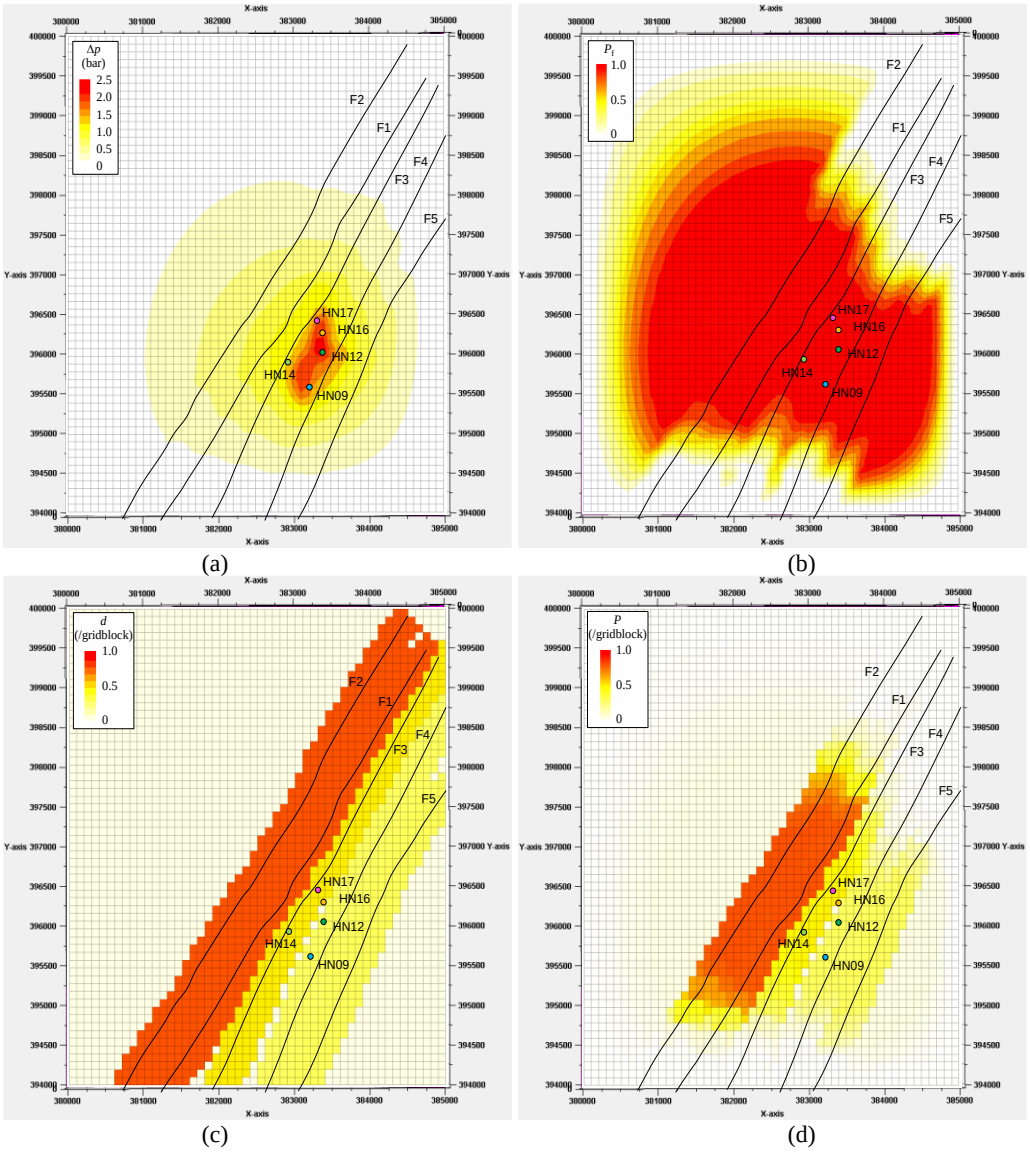

Figure 6: Susceptibility to fluid injection-induced seismicity estimated based on statistics of fracture criticality at 1 km depth at the Húsmúli area for the next six-month fluid re-injection period (16 October 2020 – 15 April 2021): (a) spatial distribution of modelled re-injection induced fluid pressure change, (b) the probability of satisfying the fracture slippage criterion, (c) the fracture density, and (d) the probability of seismic event occurrence within each gridblock. Collars for the five re-injection wells are projected to the plan view.

The probability of satisfying the fracture slippage criterion (Figure 6b) is influenced by both the fluid pressure increase driven by fluid injection operations (Figure 6a), and the intrinsic variability of fracture criticality related to the natural variability of fracture attributes and rock properties (Figure 5). This probability reaches close to 100% within a large proportion of the model domain, including F3 and F4 fault zones with a $\Delta p/h$ greater than 1.0 bar/km, F1, F2 and F5 fault zones with a $\Delta p/h$ greater than 0.5 bar/km, and off-fault zones with a $\Delta p/h$ greater than 0.3 bar/km (Figure 6a). Influenced by both the likelihood of satisfying the fracture slippage criterion (Figure 6b) and regional fracture density related to neighbouring major faults (Figure 6c), relatively high probability of seismic event occurrence was estimated for fault zones around the five re-injection wells (Figure 6d). The fracture density in off-fault zones was estimated as fairly low owing to the much less active induced seismicity in these zones during the first six-month period, therefore, the forecasted seismic susceptibility for these zones during the second six-month period was close to 0.

4.4 Comparison of six-month seismicity occurrence probability forecasts against recorded seismicity

Figure 7 presents the forecasted likelihood of seismicity occurrence within each gridblock for four subsequent six-month injection periods at 1 km reservoir depth, respectively. Field monitored seismic events during the first three six-month periods are plotted on both graphs for comparison. According to the forecasts, seismically active regions extend from fault zones F1 and F2 during October 2020 – April 2021, to fault zone F3 during April – October 2021, and gradually shrink to fault zones F3 and F5 during April – October 2022. The maximum forecasted seismicity occurrence likelihood is estimated to be reached during the period April – October 2021. Assuming that the fluid injection operational conditions remain unchanged, the forecasts suggest a seismic quiescence period during April – October 2022, owing to a much reduced seismic event count recorded (representing the intensity of potentially vulnerable underlying fractures) during the previous six-month period.

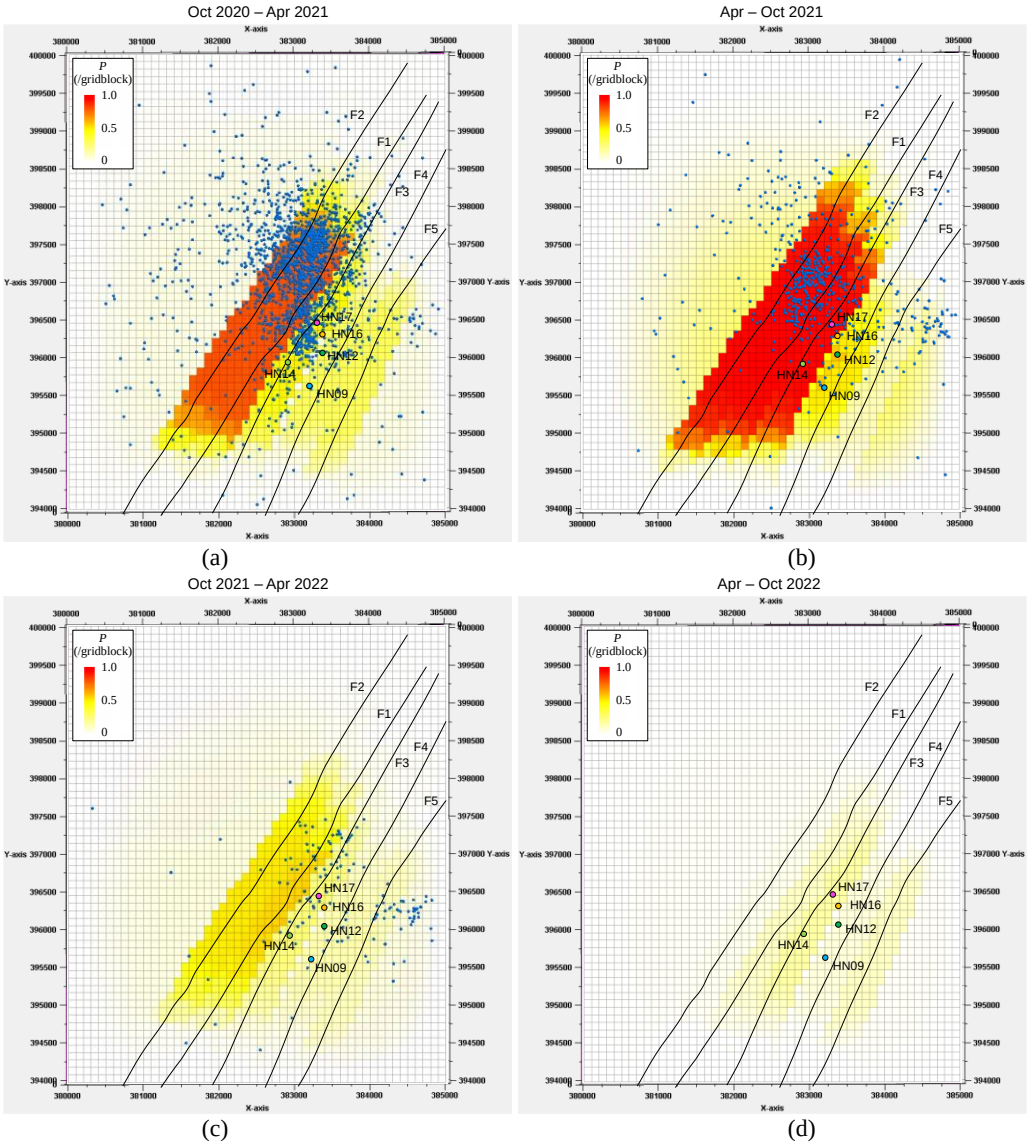

Figure 7: Six-month fluid injection-induced seismicity occurrence probability forecasts based on the statistics of fracture criticality at 1 km depth at the Húsmúli area (October 2020 – April 2021, April – October 2021, October 2021 - April 2022, and April 2022 – October 2022). Blue circles show seismicity recorded in the first three six-month periods of the forecast. Collars for the five re-injection wells are projected to the plan view.

Overall, the areas estimated to have high seismic susceptibility are fairly consistent with the seismically-active areas during the periods of investigation. The majority of induced seismicity is observed to cluster within fault zones neighbouring the re-injection wells, whilst much less seismic events are sparsely distributed in off-fault zones and fade off away from the re-injection wells. During October 2020 – April 2021, most induced seismicity is observed to fall within regions with an elevated fluid pressure in excess of 0.2 bar, in comparison with Figure 6a. The period October 2020 – April 2021 observes relatively intensive seismicity located within off-fault zones, resulting in a distinct elevation in the forecasted seismicity occurrence likelihood within these zones during April – October 2021. It is noted that the recorded seismicity is predominantly located at the northeast end of the forecasted seismically-active regions, with few occurring at the southwest end. This deviation indicates that the fault zones assumed to be homogenous in terms of hydraulic conductivities are most likely heterogeneous, forming fluid pathways from the re-injection wells towards the northeast direction but not the southwest direction.

5. DISCUSSION

Evaluation of fracture criticality combined with recorded seismicity allows for quantifying the seismotectonic state of injection sites, which is a measure of the level of seismic activity at injection sites when subjected to certain stress or pressure perturbations (Dinske and Shapiro, 2013). In this work, the seismotectonic state Ω is defined as the intensity of induced seismicity N_u (the seismic event count per unit area) divided by the fracture criticality (the critical value to trigger seismicity), i.e., $\Omega = \dfrac{N_u}{\Delta p_c / h}$. The evolution of the seismotectonic state of different regions over the four six-month injection periods of investigation is presented in Figure 8. It can be seen that the seismotectonic states vary to a large extent depending on the region and the time. During the four periods, the seismotectonic state of F1 and F2 fault zones is the most critical, followed by that of F3 and F5 fault zones, whilst that of the F4 fault zone is relatively lower. In comparison, seismotectonic state of off-fault zones is the least critical. Whilst F1, F2 and F3 fault zones

evolved seismotectonically from an active state during the first two six-month periods to a much suppressed state during the last two six-month periods, the seismotectonic state of F4 and F5 fault zones and off-fault zones maintained fairly low levels throughout.

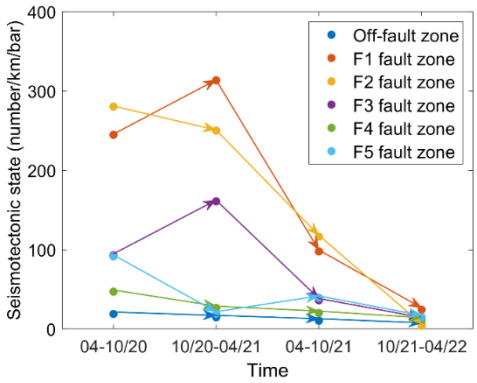

Figure 8: Evolution of the seismotectonic state of different regions (F1-F5 and off-fault zones) at Húsmúli.

It is noteworthy that, although the fracture criticality of off-fault zones may be lower than that of faulted zones (fractures are more susceptible to fluid pressure changes) (Figure 5), the fairly low density of seismicity observed at off-fault zones (Figure 6c) leads to an overall less critical seismotectonic state of off-fault zones (Figure 8) and consequently low estimated susceptibility to seismicity (Figure 6d). The seismotectonic state estimated for each region during each six-month modelling period (Figure 8) is generally consistent with the seismic susceptibility forecasted based on the statistics of fracture criticality (Figure 7).

The seismic occurrence probability forecasted is influenced by both the spatial distribution of fluid pressure change and the density of underlying fractures (Equation (3)). In this work, the fluid circulation at the Hellisheiði geothermal site has reached steady-state flow conditions during the periods of investigation, therefore, the estimated probability for induced seismicity is predominantly influenced by the varying abundance of potentially vulnerable underlying fractures under the influence of prevailing stress and fluid pressure over the fluid injection period. Nevertheless, this probabilistic seismic evaluation method is also applicable to scenarios with rapid-changing fluid pressures (e.g., increasing injection rate, cyclic injection operations, and transient shut-in), provided that the spatiotemporal evolution of fluid pressure change can be faithfully captured by the hydrogeological modelling. In this regard, the methodology proposed can be used to evaluate future fluid injection scenarios and to identify optimal operation conditions.

6. CONCLUSIONS

Based on statistics of the fracture criticality, a probabilistic seismic susceptibility evaluation framework was developed to evaluate the potential for fluid injection-induced seismicity in both faulted and off-fault reservoirs by combining seismic observations and hydrogeological simulation. The framework considers the fluid pressure increase driven by fluid injection operations, the intrinsic variability of fracture criticality, and regional fracture density related to neighbouring fault structures. This methodology was applied to evaluate susceptibility to induced seismicity at the Hellisheiði site, and relatively high probability of seismic event occurrence was estimated for fault zones around the five re-injection wells. Areas of high estimated fracture slip susceptibility experienced high levels of induced seismicity over the fluid re-injection period of investigation. During the 2-year re-injection period investigated, whilst F1, F2 and F3 fault zones evolved seismotectonically from an active state during the first two six-month periods to a much suppressed state during the last two six-month periods, the seismotectonic state of F4 and F5 fault zones and off-fault zones maintained fairly low levels throughout. The seismotectonic state estimated for each region during each six-month modelling period is generally consistent with the seismic susceptibility forecasted based on the statistics of fracture criticality.

ACKNOWLEDGEMENTS

This research was carried out as part of the project “Synergetic Utilisation of CO_2 storage Coupled with geothermal Energy Deployment - SUCCEED” funded through the ACT programme (Accelerating CCS Technologies, Horizon 2020 Project No 294766). Financial contributions made by the Department for Business, Energy & Industrial Strategy UK, the Ministry of Economic Affairs and Climate Policy, the Netherlands, the Scientific and Technological Research Council of Turkey are gratefully acknowledged. The authors also wish to thank the Swiss Seismological Service (SED) at ETH Zurich for their permission to use the Hengill (Iceland) seismic monitoring data from the COSEISMIQ network (http://networks.seismo.ethz.ch/en/networks/2c/).

REFERENCES

Cao, W., Durucan, S., Cai, W., Shi, J.-Q., & Korre, A. A physics-based probabilistic forecasting methodology for hazardous microseismicity associated with longwall coal mining. *International Journal of Coal Geology*, 232, (2020), 103627.

Cao, W., Durucan, S., Cai, W., Shi, J.-Q., Korre, A., Jamnikar, S., et al. The role of mining intensity and pre-existing fracture attributes on spatial, temporal and magnitude characteristics of microseismicity in longwall coal mining. *Rock Mechanics and Rock Engineering*, 53, (2020), 4139–4162.

Cao, W., Durucan, S., Shi, J.-Q., Cai, W., Korre, A., Ratouisc, T. Induced seismicity associated with geothermal fluids re-injection: Poroelastic stressing, thermoelastic stressing, or transient cooling-induced permeability enhancement? *Geothermics*, 102, (2022), 102404.

Dinske, C., & Shapiro, S. A. Seismotectonic state of reservoirs inferred from magnitude distributions of fluid-induced seismicity. *Journal of Seismology*, 17(1), (2013), 13–25.

Elsworth, D., Spiers, C. J., & Niemeijer, A. R. Understanding induced seismicity. *Science*, 354(6318), (2016), 1380–1381.

Fisher, M. K., Heinze, J. R., Harris, C. D., Davidson, B. M., Wright, C. A., & Dunn, K. P. Optimizing horizontal completion techniques in the Barnett shale using microseismic fracture mapping. In *SPE Annual Technical Conference and Exhibition*. OnePetro (2004).

Frolova, J., Franzson, H., Ladygin, V., Sigurdsson, O., Stefánsson, V., & Shustrov, V. Porosity and permeability of hyaloclastites tuffs, Iceland. In *Proceedings of International Geothermal Workshop IGW2004 "Heat and light from the heart of the earth* (2004).

Grigoli, F., Cesca, S., Priolo, E., Rinaldi, A. P., Clinton, J. F., Stabile, T. A., et al. Current challenges in monitoring, discrimination, and management of induced seismicity related to underground industrial activities: A European perspective. *Reviews of Geophysics*, 55(2), (2017), 310–340.

Gunnarsdóttir, S. H., & Poux, B. 3D Modelling of Hellisheiði Geothermal Field using Leapfrog: Data, Workflow and Preliminary Models. *Report ÍSOR-2016* (2016).

Gunnarsson, G. Temperature Dependent Injectivity and Induced Seismicity–Managing Reinjection in the Hellisheiði Field, SW-Iceland. *GRC Transactions*, 37, (2013), 1019–1025.

Juncu, D., Árnadóttir, T., Geirsson, H., Guðmundsson, G. B., Lund, B., Gunnarsson, G., et al. Injection-induced surface deformation and seismicity at the Hellisheidi geothermal field, Iceland. *Journal of Volcanology and Geothermal Research*, 391, (2020), 106337.

Ratouis, T. M. P., Snæbjörnsdóttir, S. O., Gunnarsson, G., Gunnarsson, I., Kristjánsson, B. R., & Aradóttir, E. S. P. Modelling the Complex Structural Features Controlling Fluid Flow at the CarbFix2 Reinjection Site, Hellisheiði Geothermal Power Plant, SW-Iceland. In *44th Workshop on Geothermal Reservoir Engineering* (2019).

Rothert, E., & Shapiro, S. A. Statistics of fracture strength and fluid‐induced microseismicity. *Journal of Geophysical Research: Solid Earth*, 112(B4), (2007).

Schultz, R., Beroza, G. C., & Ellsworth, W. L. A Strategy for Choosing Red‐Light Thresholds to Manage Hydraulic Fracturing Induced Seismicity in North America. *Journal of Geophysical Research: Solid Earth*, 126(12), (2021), e2021JB022340.

Shapiro, S. A. Fluid-induced seismicity. *Cambridge University Press* (2015).

Snæbjörnsdóttir, S. Ó., Wiese, F., Fridriksson, T., Ármansson, H., Einarsson, G. M., & Gislason, S. R. CO2 storage potential of basaltic rocks in Iceland and the oceanic ridges. *Energy Procedia*, 63, (2014), 4585–4600.

Snæbjörnsdóttir, S. Ó., Tómasdóttir, S., Sigfússon, B., Aradóttir, E. S., Gunnarsson, G., Niemi, A., et al. The geology and hydrology of the CarbFix2 site, SW-Iceland. *Energy Procedia*, 146, (2018), 146–157.

Tómasdóttir, S. Flow Paths in the Húsmúli Reinjection Zone, Iceland (2018).

Walsh III, F. R., & Zoback, M. D. Probabilistic assessment of potential fault slip related to injection-induced earthquakes: Application to north-central Oklahoma, USA. *Geology*, 44(12), (2016), 991–994.

Zhang, Y., Person, M., Rupp, J., Ellett, K., Celia, M. A., Gable, C. W., et al. Hydrogeologic controls on induced seismicity in crystalline basement rocks due to fluid injection into basal reservoirs. *Groundwater*, 51(4), (2013), 525–538.

Zhao, Y., Yang, T., Zhang, P., Xu, H., Zhou, J., & Yu, Q. Method for generating a discrete fracture network from microseismic data and its application in analyzing the permeability of rock masses: a case study. *Rock Mechanics and Rock Engineering*, 52(9), (2019), 3133–3155.